2021 43rd Annual International Conference of the
IEEE Engineering in Medicine & Biology Society (EMBC)
Oct 31 - Nov 4, 2021. Virtual Conference

Evaluation of the RF-induced lead-tip heating of AIMDs using a Volume-Weighed Tissue-Cluster Model for 1.5T MRI

Ran Guo, Jianfeng Zheng, *Member, IEEE*, Meiqi, Xia, Guangqiang Jiang, Devashish Shrivastava, Wolfgang Kainz, *Member, IEEE*, and Ji Chen, *Senior Member, IEEE,*

***Abstract*— The RF-induced lead-tip heating of AIMDs is related to the tangential electric field distribution along the AIMD lead paths in patients and the electromagnetic behavior (represented by the transfer function model) of the AIMDs. To evaluate the *in-vivo* RF-induced lead-tip heating of AIMDs using *in-vitro* methods, the electric field distribution is critical. In this paper, we proposed a Volume-Weighed Tissue-Cluster Model, a feasible bench method, to simplify the evaluation of the *in-vivo* RF-induced lead-tip heating of AIMDs. The incident electric field distribution inside this simplified model is highly correlated to that of the original inhomogeneous human body model. Compared to the RF-induced lead-tip heating results in the original model, the maximum error of the lead-tip heating in this Volume-Weighed Tissue-Cluster Model is less than 1 ℃. The correlation coefficients of the temperature rise between the two models are higher than 0.997.**

***Clinical Relevance*— Simplified and accurate anatomical models can be used to emulate the in-vivo heating assessment for MRI safety.**

I. Introduction

The RF-induced heating hazards for patients with the active implantable medical device (AIMD) during magnetic resonance imaging (MRI) have been widely studied in decades [1]. Currently, researchers often use a Tier 3-compliant method from ISO 10974-2-33 [2] to evaluate the RF-induced heating for general AIMDs. For the Tier 3-compliant method, the two essential input factors are the validated AIMD models, named transfer functions, and the incident tangential electric field along the clinically relevant AIMD trajectories in patient bodies.

To accurately evaluate the RF-induced heating of AIMDs, including the characteristics with the device configurations and clinical conditions, the *in-vivo* incident field distribution should be considered. However, due to the difficulty in the direct measurement of the *in-vivo* temperature rise, it is necessary to consider other methods, such as the computational methods, that can emulate the measured values from *in-vivo* cases. For electric field distribution within human bodies, the electric field distribution is related to human body geometry, tissue electrical properties, and inhomogeneous tissue distributions inside the human body. Hence, these factors should have a large effect on the RF-induced heating evaluation.

Previous studies on RF-induced heating in phantom have already considered the tissue effect [3]. The results indicated that the tissue electrical properties have a strong impact on RF-induced heating. However, in the gel-phantom studies, the tissue distribution and phantom shape in their studies are different from the real human body models Therefore, in this study, we propose a Volume-Weighing Tissue-Cluster (VWC) Model, a potential *in-vitro* method to evaluate the *in-vivo* RF-induced heating of AIMDs.

The proposed VWC model is based on the Gaussian mixture model (GMM) of ε_r and $\frac{\sigma}{\omega\varepsilon_0}$ developed using tissue electrical permittivity and conductivity values. Three representative human models, Duke (adult male), Ella (adult female), and Obese (adult obese male) from the virtual family projects [4], were used to establish the GMM for the VWC model with 1 to 8 different clusters. The correlation coefficients of incident electric field distributions in several selected regions were used as a criterion to determine the number of clusters. Based on the study, the VWC model with k=2 clusters (VWCk2) is selected for further RF-induced heating evaluation. The RF-induced heating of an SNM device was conducted in normal and VWCk2 models. Compared to the RF-induced heating results in the original model, the maximum error of the results in this VWCk2 is less than 1 ℃. The correlation coefficients of the temperature rise between the two models are higher than 0.997.

II. Methods

A. Tissue properties in the human model

The electrical properties of each tissue inside the human model are already given in the standard ISO 10974-2-33. Generally, the relative permittivity value ranges from 0 to 118.56 (Kidney). And the electric conductivity value ranges

Ji Chen is with the ECE department at University of Houston, Houston, TX 80305 USA (phone: 713-743-4423; e-mail: jchen18@uh.edu). Ran Guo, Jianfeng Zheng, and Meiqi Xia were with University of Houston, Houston, TX 77005 USA. (e-mail: guoran188@gmail.com; jason.zhjf@gmail.com, meiqixia9@gmail.com). Guangqiang Jiang is with Axonics, Inc., 26 Technology Dr., Irvine CA 92618 (e-mail: gjiang@axonics.com). Devashish Shrivastava and Wolfgang Kainz is with Center for Devices and Radiological Health, Food and Drug Administration, Silver Spring, MD 20993, USA (e-mail: devashish.shrivastava@fda.hhs.gov; Wolfgang.Kainz@fda.hhs.gov).

from 0 S/m to 2.07 S/m (Cerebrospinal fluid). The scatter plot for conductivity and permittivity of all tissues is shown in Fig. 1.

Combine the conductive and displacement parts and take ε_0 outside, we can have

$$\nabla \times \vec{H} = \vec{J_i} + j\omega\varepsilon_0(\varepsilon_r - j\frac{\sigma}{\omega\varepsilon_0})\vec{E} \qquad (1)$$

where ε_r is the relative permittivity for each tissue, σ is the conductivity for each tissue, ω is the radian frequency, and ε_0 is constant of vacuum permittivity. Considering 1.5T (64MHz) MRI conditions, the scatter plot of ε_r and $\frac{\sigma}{\omega\varepsilon_0}$ is shown in Fig. 2.

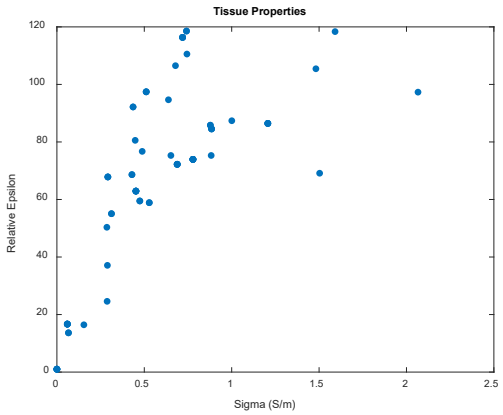

Fig. 1. The scatter plot for conductivity and permittivity of all tissues

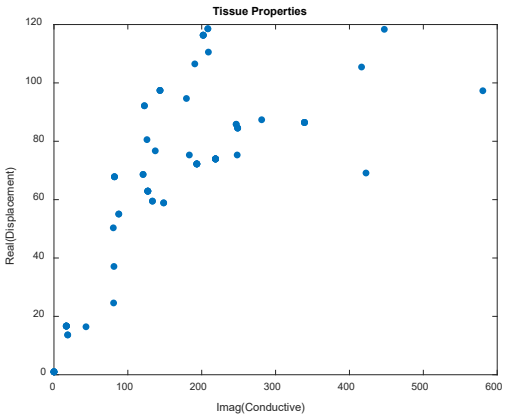

Fig. 2. The scatter plot for ε_r and $\frac{\sigma}{\omega\varepsilon_0}$ of all tissues

B. GMM calculation for VWC model

The volume-weighted ε_r and $\frac{\sigma}{\omega\varepsilon_0}$ are calculated for each model. The entire numerical model is meshed into grid cells with a unit one of 2 mm × 2 mm × 2 mm. The volume-weighted ε_r and $\frac{\sigma}{\omega\varepsilon_0}$ are calculated as $\varepsilon_r = \sum_{i=1}^{N} \varepsilon_{ri} M_i$ and $\frac{\sigma}{\omega\varepsilon_0} = \sum_{i=1}^{N} \frac{\sigma_i}{\omega\varepsilon_0} M_i$. M_i is the total occurrence of *i-th* tissue type. ε_r and σ_i are the tissue conductivity for *i-th* type.

With the volume-weighted ε_r and $\frac{\sigma}{\omega\varepsilon_0}$, the Gaussian mixture model (GMM) is generated. The Akaike Information Criterion (AIC) and Bayesian Information Criterion (BIC) are calculated to determine the number of components. Initially, a total of 8 components are considering in GMM. Fig. 3(A) shows the VWC model for k=8 clusters. Based on the AIC and BIC results for all k=1 to k=8 clusters and the consideration of model simplicity, the VWC model of k=2 clusters is finally selected, as shown in Fig. 3(B).

C. Numerical simulation for the incident electric field

Full-wave electromagnetic simulation software SEMCAD X, based on the Finite Difference Time Domain (FDTD) algorithm, is used for the numerical simulations. A non-physical birdcage coil is modeled and used in numerical simulations. The coil has a diameter of 630 mm and a height of 650 mm. This coil represents a typical RF coil for MRI systems. A circular polarized electromagnetic field is generated inside the birdcage coil excited by 8 sources at the rungs. At the excitation locations, continuous sinusoidal signals of the same magnitude and a phase increment of π/4 along the clockwise direction are used.

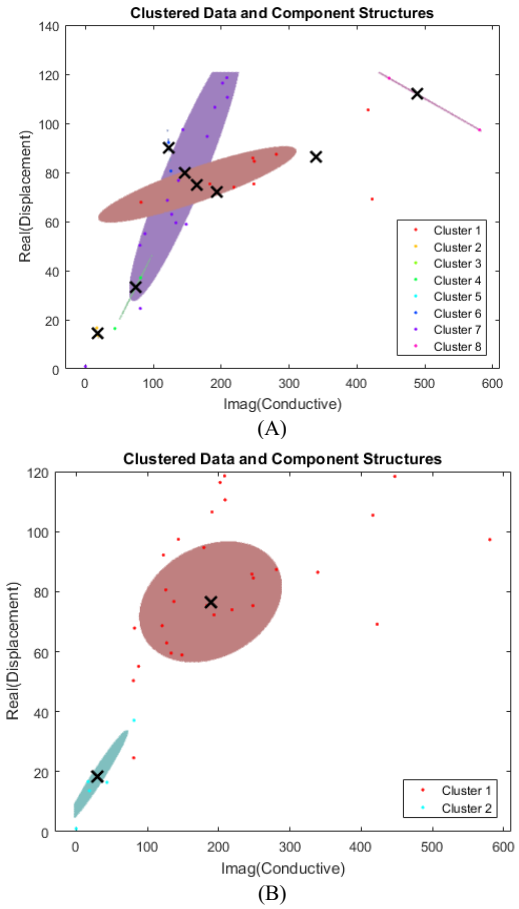

Fig. 3. The VKC model for (A) k=8 and (B) k=2 clusters.

Graphics Processing Unit (GPU) hardware acceleration is achieved using the SPEAG CUDA library with Nvidia GeForce GTX1080 graphic card, which provided a computation capability of 1500 million cells per second. The mesh size for the human body is 2 mm. The total number of cells is less than 70 Million Cells in most simulations. To assure convergence of the numerical simulations, the

simulation time is set to 20 periods for each simulation, and convergence analysis is performed after each simulation.

The virtual human models are loaded into the RF coil with a head-in direction. The relative position of the patient inside the MRI bore to the center of the MRI coil is defined as the landmark positions. To include all potential scanning positions, the model was simulated using 9 landmark positions (using a 200 mm step size and spanning 1600 mm along the axis of the bore). The landmarks ranging from -200 mm to 1400 mm are considered in this study. The landmark 0 mm is corresponding to the center of the eyes at the center of the MR coil and the landmark 1400 mm corresponds to the position where the knee is located at the center of the coil for the adult model.

Sacral neuromodulation (SNM) system lead pathways for each Virtual Population model are defined and developed based on the X-ray images of lead trajectories from patients who have the SNM implants during the clinical trials. The pathway trajectories in the adult male model are shown in for example. The 300 mm stimulation lead could be inserted through sacral foramen on either the left or right side. The proximal and distal positions are considered for the neurostimulator, which is around the upper buttock area. To test the effect of the lead geometrical deviation, these 24 lead pathways are shifted from the original trajectory in each direction one at a time by 2 or -2 mm to obtain, in total, up to seven variations (including the original one) for each trajectory, resulting in 168 pathways in total in each model.

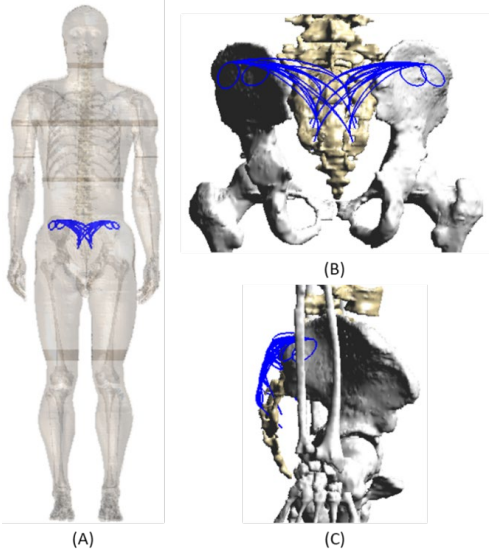

Fig. 4. Virtual trajectories for the Duke model (A); Enlarged view of the trajectories and their relative position with vertebrae (B)(C).

D.RF-induced heating calculation

The transfer function method is applied to evaluate the RF-induced heating for the SNM implants. Feng et al proposed a measurement method for the transfer function based on the Reciprocity Theorem [5]. The transfer function is a complex that is proportional to the common mode current along the lead when a fixed source is applied at the tip of the implant. With a known TF, the electric field at the tip is calculated using:

$$\vec{E}_{tip} = \int_L \frac{I_L(l) \cdot \vec{E}_{inc}(l) \cdot \vec{l}\, dl}{I_{tip} L_I} = \alpha \int_L F(l) \cdot E_{inc}(l)\, dl \quad (3)$$

where $\vec{E}_{tip}$ is the electric field near the tip of the implant, $I_{tip}L_I$ is the applied small dipole source at the tip electrode, I_L is the measured current along the implant lead body, $\vec{E}_{inc}$ is the incident electric field along the implant in the human body, which could be extracted from the numerical simulation without the implant present, and $F(l)$ is the complex transfer function. α is a scaling factor of the transfer function $F(l)$.

The temperature distribution around the tip electrode can be determined from the specific absorption rate (SAR) using a thermal model. Provided that the temperature rise is small enough that there is a minimal variation in the thermal properties, the temperature increases at a point near the lead-tip ΔT can be evaluated using:

$$\Delta T \propto SAR_{tip} = \frac{\sigma \left|\vec{E}_{tip}\right|^2}{\rho} = \alpha^2 \left| \int_L F(l) \cdot E_{inc}(l)\, dl \right|^2 \quad (4)$$

where σ and ρ are corresponding to the electrical conductivity and density of the material at the lead tip. It is shown that the temperature increase ΔT is proportional to the square of the magnitude of the electric field $\vec{E}_{tip}$ at a point near the lead-tip and inversely proportional to the value of the specific heat [6]. Thus, from the knowledge of transfer function, the incident electric field along the lead, and the material properties of the tissue around the electrode, the heating of the tissue near the electrode due to the RF field inside an MR scanner can be determined.

III. Results and Discussion

E. Tissue properties for the VWCk2 models

Based on the GMM calculation results for the VWC models, the k=2 clusters are selected for VWC simplified model. Due to the anatomy difference among Duke, Ella, and the Obese models, the volume for each tissue depends on the corresponding model. The summary of the tissue properties for the VWCk2 models is shown in Table I. It is shown that the tissues with lower permittivity and conductivity are collected into the first cluster. And the tissues with higher permittivity and conductivity are collected into the second cluster. The detailed cluster selection is shown in Fig. 3(B).

TABLE I. THE TISSUE PROPERTIES FOR THE VWCK2 MODELS.

	Cluster 1		Cluster 2	
	Fat, Bone, Marrow, …		Muscle, Skin, Blood, …	
Duke	ε=18.38	σ=0.11 S/m	ε=76.58	σ=0.67 S/m
Ella	ε=14.11	σ=0.07 S/m	ε=72.03	σ=0.63 S/m
Obese	ε=13.88	σ=0.07 S/m	ε=72.97	σ=0.63 S/m

F. Comparison for the incident electric field

The incident electric field distribution for the normal and VWCk2 models is calculated and compared. The results at

landmark 600 mm are selected for comparison. Considering the typical positions for the medical implants, the electric field in five regions is extracted for the comparison, which are left arm, right arm, left tibia, right tibia, and hip with the femur. Take the Duke model, for example, the correlation coefficients between the normal and the VWCk2 models are calculated and shown in Table II. The minimum correlation coefficient is 0.96. Furthermore, the 1g averaged SAR distributions for normal and VWCk2 Duke models are presented in Fig. 5. It shows that the distribution of the 1g averaged SAR is very similar. The error for the peak 1g averaged SAR is 3.4%.

TABLE II. THE CORRELATION COEFFICIENTS OF THE ELECTRIC FIELD IN DIFFERENT REGIONS

	E_x		E_y		E_z		E_{tot}
	Abs	Phase	Abs	Phase	Abs	Phase	Abs
Left arm	1.00	0.00	1.00	0.00	1.00	0.00	1.00
Right arm	0.99	0.03	0.99	0.02	0.99	0.01	0.99
Left tibia	0.98	-0.02	0.98	0.05	0.97	0.14	0.97
Right tibia	1.00	0.01	1.00	0.00	0.96	0.11	0.99
Hip with femur	0.99	-0.01	0.99	0.00	1.00	-0.04	0.99

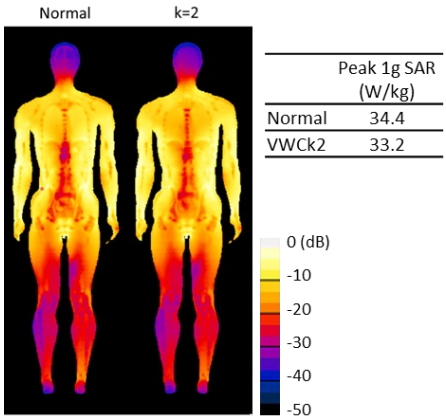

Fig. 5. The 1g averaged SAR distribution in the normal and VWCk2 Duke models

G. Comparison of the RF-induced heating

The RF-induced heating for the SNM devices is calculated for both the normal and the VWCk2 models of Duke, Ella, and the Obese model. The simulation results are normalized to the Normal Operating Mode (IEC 60601-2-33) limits. The transfer functions of SNM devices include two different mediums and two tip electrodes. With 168 lead pathways in each human model, a total of 672 cases are considered for each landmark and 6048 cases for each human model.

With the calculated RF-induced lead-tip heating results, the correlation coefficients between the normal and the VWCk2 models are calculated for Duke, Ella, and Obese. The scattering plots are shown in Fig. 6. The correlation coefficient equals higher than 0.997 for all three models. The maximum error of the lead-tip temperature rise between the normal and the VWCk2 models is less than 0.6 ℃. It is shown that at least 85% of cases have an absolute error of less than 0.2 ℃.

IV. CONCLUSION

In this paper, we propose a VWCk2 Model, a feasible *in-vitro* method, to evaluate the *in-vivo* RF-induced lead-tip heating of AIMDs. The incident electric field in this model is highly correlated to the original in the human body model. Comparing the RF-induced heating results to the original human body model, the maximum error of the lead-tip heating using the VWCk2 model is less than 0.6 ℃. The correlation coefficients of the temperature rise between the two models are higher than 0.997.

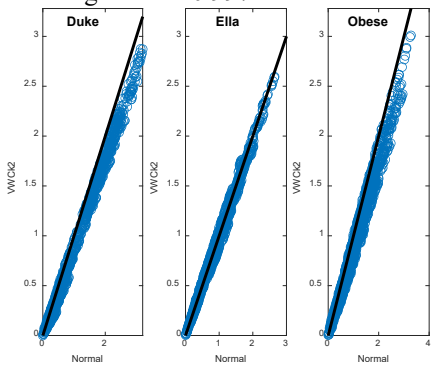

Fig. 6. The scattering plot for the temperature rise in normal and VWCk2 models for Duke, Ella, and Obese.

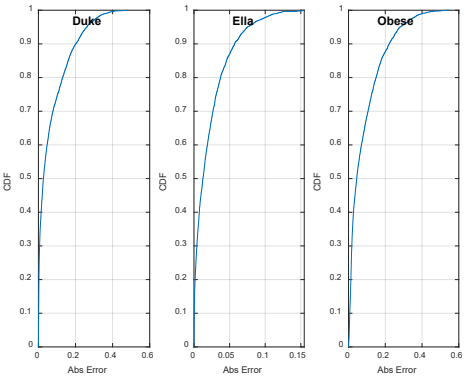

Fig. 7. The cumulative distribution function of the temperature increment absolute error between the normal and VWCk2 models.

V. REFERENCES

[1] Q. Zeng, Q. Wang, J. Zheng, W. Kainz, and J. Chen, "Evaluation of MRI RF electromagnetic field induced heating near leads of cochlear implants," Phys. Med. Biol., vol. 63, no. 13, 2018, doi: 10.1088/1361-6560/aacbf2.

[2] ISO/TS 10974. "Assessment of the safety of magnetic resonance imaging for patients with an active implantable medical device." International Organization for Standarization (2018).

[3] R. Guo, J. Zheng, and J. Chen, "Comparison of in-vivo and in-vitro MRI RF heating for orthopedic implant at 3 tesla," 2017, doi: 10.1109/APUSNCURSINRSM.2017. 8072552.

[4] A. Christ et al., "The Virtual Family - Development of surface-based anatomical models of two adults and two children for dosimetric simulations," Phys. Med. Biol., 2010, doi: 10.1088/0031-9155/55/2/N01.

[5] S. Feng, R. Qiang, W. Kainz, and J. Chen, "A technique to evaluate MRI-induced electric fields at the ends of practical implanted lead," IEEE Trans. Microw. Theory Tech., vol. 63, no. 1, pp. 305–313, 2015, doi: 10.1109/TMTT.2014.2376523.

[6] Shrivastava D (Editor), Theory and Applications of Heat Transfer in Humans, John Wiley & Sons, 2018.